Technology

Molecular Cell

Large-Scale, Quantitative Protein Assays on a High-Throughput DNA Sequencing Chip

Graphical Abstract

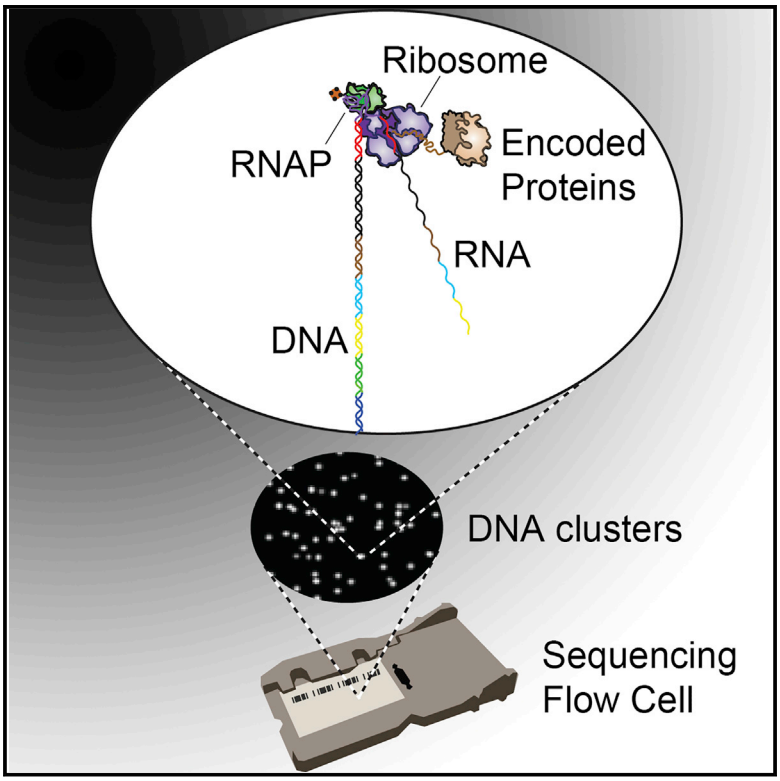

Authors

Curtis J. Layton, Peter L. McMahon, William J. Greenleaf

Correspondence

wjg@stanford.edu

In Brief

By generating a massive peptide and protein array *in situ* on an Illumina sequencing flow cell with *in vitro* translation, Layton et al. demonstrate direct protein assays for enzyme function and antibody-peptide interactions across large libraries ($\sim 10^5$) of mutational variants on an automated platform.

Highlights

- Generation of a massive peptide and protein array on a sequencing flow cell
- Direct measurement of binding and catalysis for $\sim 10^5$ protein mutational variants
- Patterns of amino acid mutation and cooperativity were analyzed in high throughput
- Discovery of high-avidity "superFLAG" epitope for the M2 anti-FLAG antibody

Layton et al., 2019, Molecular Cell *73*, 1075–1082
March 7, 2019
https://doi.org/10.1016/j.molcel.2019.02.019

CellPress

Molecular Cell
Technology

Large-Scale, Quantitative Protein Assays on a High-Throughput DNA Sequencing Chip

Curtis J. Layton,[1] Peter L. McMahon,[2] and William J. Greenleaf[1,2,3,4,*]
[1]Department of Genetics, Stanford University School of Medicine, Stanford, CA 94305, USA
[2]Department of Applied Physics, Stanford University, Stanford, CA 94305, USA
[3]Chan-Zuckerberg Initiative, Palo Alto, CA 94301, USA
[4]Lead Contact
*Correspondence: wjg@stanford.edu
https://doi.org/10.1016/j.molcel.2019.02.019

SUMMARY

High-throughput DNA sequencing techniques have enabled diverse approaches for linking DNA sequence to biochemical function. In contrast, assays of protein function have substantial limitations in terms of throughput, automation, and widespread availability. We have adapted an Illumina high-throughput sequencing chip to display an immense diversity of ribosomally translated proteins and peptides and then carried out fluorescence-based functional assays directly on this flow cell, demonstrating that a single, widely available high-throughput platform can perform both sequencing-by-synthesis and protein assays. We quantified the binding of the M2 anti-FLAG antibody to a library of 1.3 × 10^4 variant FLAG peptides, exploring non-additive effects of combinations of mutations and discovering a "superFLAG" epitope variant. We also measured the enzymatic activity of 1.56 × 10^5 molecular variants of full-length human O^6-alkylguanine-DNA alkyltransferase (SNAP-tag). This comprehensive corpus of catalytic rates revealed amino acid interaction networks and cooperativity, linked positive cooperativity to structural proximity, and revealed ubiquitous positively cooperative interactions with histidine residues.

INTRODUCTION

High-throughput DNA sequencing technologies have enabled the investigation of diverse biological processes wherein the functional consequences of nucleic acid variation can be linked directly to the abundance and sequence of DNA fragments that are quantified at scale. These applications (e.g., ChIP-seq, ATAC-seq, bisulfite sequencing, Hi-C, bind-n-seq, etc. [Park, 2009; Buenrostro et al., 2013; Krueger et al., 2012; Lieberman-Aiden et al., 2009; Zykovich et al., 2009]) largely define the contemporary methodological foundations of modern functional genomics. In contrast, methods for directly assaying the influence of protein sequence variation on function have remained challenging to similarly scale and disseminate (Kingsmore, 2006). *In vitro* approaches for high-throughput protein functional measurements have included the quantification of selective enrichment (Larman et al., 2011; Fowler et al., 2010; Gu et al., 2014) of protein particles linked to their encoding nucleic acids (Levin and Weiss, 2006; Odegrip et al., 2004) and parallelized binding assays on protein and peptide microarrays (Chandra et al., 2011), including arrays generated with *in vitro* protein translation (He et al., 2008; Ramachandran et al., 2004; Tao and Zhu, 2006) and *in situ* peptide synthesis (Hilpert et al., 2007; Legutki et al., 2014; Forsström et al., 2014). However, existing implementations have not yet provided the scalability, simplicity, automation, or accessibility necessary for widespread application. The implementation of direct and quantitative assays of protein function with the automation and throughput of a modern high-throughput sequencing platform would greatly expand our ability to develop and test a predictive understanding of the functional impact of coding mutations, to identify and characterize amino acid interaction networks and dependencies, and to learn useful principles and paradigms for rational design of protein function.

DESIGN

To enable straightforward, widely deployable, high-throughput, and quantitative protein characterization, we sought to leverage the capabilities and widespread adoption of the now-ubiquitous DNA-sequencing flow cells to directly assay protein function at scale. High-throughput flow cell DNA arrays, the core of Illumina sequencing (Bentley et al., 2008), have recently been repurposed for quantitative high-throughput investigation of DNA-protein, RNA-protein, and RNA-RNA interactions across nucleic-acid sequence space. Building on this and other work (Nutiu et al., 2011; Tome et al., 2014; Buenrostro et al., 2014; She et al., 2017; Svensen et al., 2016; Gu et al., 2014) we have reengineered high-throughput DNA-sequencing methods to assay protein function across a vast polypeptide sequence space. This approach aims to bring quantitative protein functional investigation to DNA-sequencing-scale throughput using a hardware platform and microfluidic chip compatible with fluorescence-based sequencing by synthesis (SBS) methods, demonstrating that a single, widely available high-throughput platform can, in principle, perform both sequencing-by-synthesis and protein function assays.

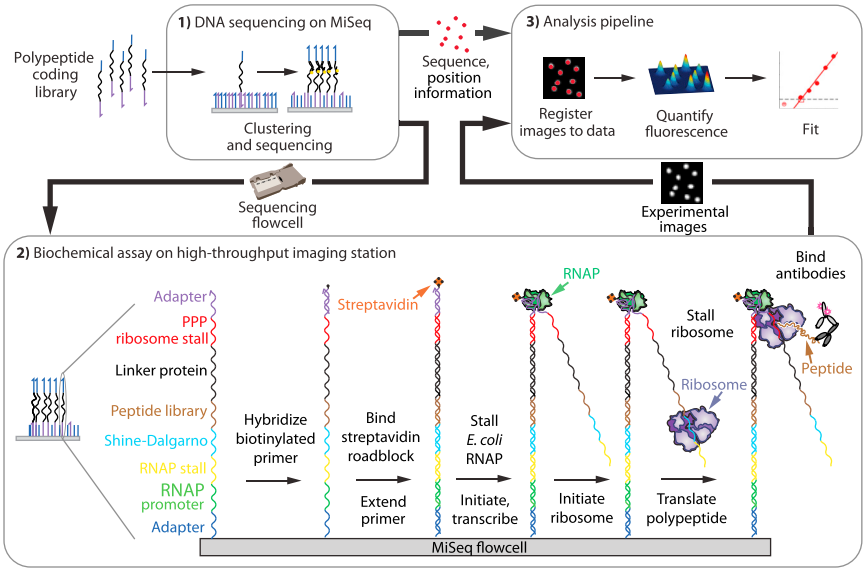

Figure 1. A High-Throughput Protein Array on a DNA Sequencing Flow Cell

(1) A polypeptide-encoding DNA library is clustered and sequenced on a MiSeq. Then the chip is transferred to an imaging station, where (2) roadblocked transcription and stalled translation takes place *in vitro*, producing bound polypeptides. Protein functional assays can then be performed on all displayed variants, such as interrogation with a primary antibody and fluorescently labeled secondary antibody (shown) followed by fluorescence imaging. (3) Fluorescence images are registered to the sequence information, then quantified and fit.

To develop methods capable of generating and quantifying our protein array on an SBS-compatible platform, we constructed a flexible, programmable workstation capable of microfluidically interfacing with and imaging sequencing flow cells (Jung et al., 2017; She et al., 2017). The resulting TIRF microscopy platform, based on the automated fluidics and fluorescence microscopy components of an Illumina GAIIx sequencer, interfaces with previously sequenced (and therefore sequence- and position-indexed) Illumina MiSeq flow cell arrays (She et al., 2017). To generate a protein array, we create a library of engineered DNA constructs that encode for polypeptides of interest (Figure S1) and then sequence this library on an Illumina MiSeq. After moving the sequenced chip to our assay platform, we re-register the cluster positions to their sequences (see STAR Methods). We next perform *in vitro* transcription/translation on chips such that both the transcript and nascent peptide remain associated with their DNA template, producing a tethered protein array. To enable this tethered display, each member of the sequencing library contains DNA sequence elements that allow for (1) prokaryotic *in vitro* transcription, (2) immobilization of the resulting RNA transcript, (3) translation, and (4) ribosome stall, similar to ribosome display (Lipovsek and Plückthun, 2004) (Figure 1). Fluorescence-based functional assays (e.g., quantifying binding of fluorescently labeled binding partners or incorporation of fluorescent substrates) may then be conducted directly on this array. Fluorescence images, paired to cluster DNA sequences generated from the sequencing run, are then quantified (see STAR Methods) to assay polypeptide binding or other protein function. We call this method *prot*ein display on a *m*assively *p*arallel array, or Prot-MaP.

RESULTS

As a testbed for this methodology, we characterized the widely used FLAG peptide/M2 antibody interaction. FLAG peptide (canonically DYKDDDDK) is commonly used for protein labeling and purification and as a general affinity reagent (Einhauer and Jungbauer, 2001). The consensus sequence profile of the linear peptide epitope of M2 has previously been characterized as DYKxxDxx based on 5 (Srila and Yamabhai, 2013) or 18 (Osada et al., 2009) clones selected from random peptide libraries. We aimed to generate a library of target peptides that would comprehensively probe the contribution of residues in the FLAG peptide to the M2 antibody interaction with a much larger library of variants. We engineered a variant library of 13,154 sequences that encoded all single, double, and triple combinations of mutant positions, with each position substituted to each of 6 different amino acids—A, K, D, S, F, and L—that represent small, positive, negative, polar, aromatic, and aliphatic substitutions, respectively. The peptide-coding mutant library was produced with microarray synthesis and assembled into a sequenceable library construct with elements enabling transcription, translation, and stable peptide display (Figures 1 and S1; see STAR Methods).

After DNA sequencing, 623,075 total clusters encoding FLAG library members were produced with 12,739 of 13,154 (96.8%) programmed variants represented by 8 or more peptide clusters (i.e., nearly complete coverage of this synthetic FLAG library required only ~2.5% of capacity of the flow cell). After peptide generation, M2 antibody was introduced at increasing concentrations and allowed to bind to the peptide, with each concentration followed by detection with a fluorescently labeled secondary antibody, then imaging (Figure 2A). After image registration and fluorescence quantification, the limit of detection (LoD) for antibody binding was determined for each variant (Figure 2B; see STAR Methods), representing the lowest concentration of antibody that produces detectable binding. This Prot-MaP LoD assay is analogous to a massively multiplexed ELISA whereby primary antibody interactions are probed by secondary detection steps that produce measurable signal.

The single and double mutant affinity landscapes (Figures 2C and 2D) of the canonical sequence (DYKDDDDK, "WT") largely recapitulate the previously reported motif pattern, DYKxxDxx (Srila and Yamabhai, 2013; Osada et al., 2009). However, we observe substantial additional constraint at position D4, with 5 of 6 mutations exhibiting no detectable binding. To further investigate mutational constraint at this position, we asked if detrimental mutations at position 4 could be rescued by mutations

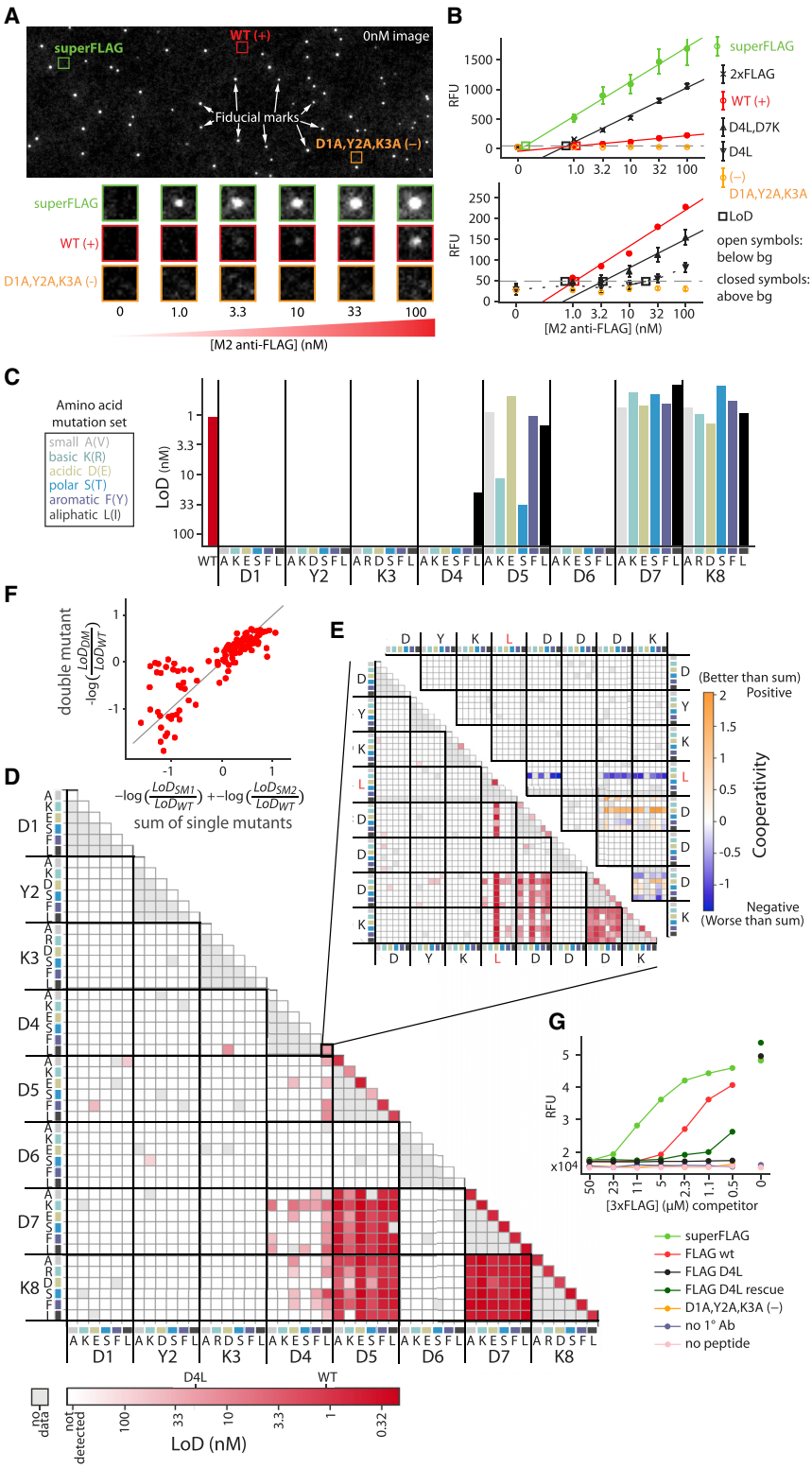

Figure 2. Binding Landscape of FLAG Peptide Variants to M2 Monoclonal Antibody

(A) A representative flow cell image shows fiducial marks and cluster-of-interest positions before the binding assay (top). Experimental images show fluorescent secondary antibody detection of binding across increasing concentrations of M2 anti-FLAG primary antibody (bottom).

(B) Quantified fluorescence medians (error bars are SEM) that rise above a background threshold (gray dashed line) are extrapolated (solid) or interpolated (dashed) to estimate the limit of detection (LoD, open squares) for each FLAG variant, including WT FLAG (DYKDDDDK) and negative control (AAADDDDK) as well as superFLAG variant (DYKDEDLL), which, like 2×FLAG (DYKDDDDKGDYKDHD), gives much higher signal than WT. Two different scales are shown (top versus bottom) to accommodate the wide dynamic range of observed signals. Open symbols indicate points below background, and closed symbols are above.

(C and D) Six amino acid mutations, each representing a physicochemical category, are represented by color (C) (if the WT identity is the same, the alternate mutation in parenthesis is made). LoD for M2 anti-FLAG antibody binding to single mutants and (D) double mutants of the canonical (WT) peptide, DYKDDDDK, across the six amino acids at each position.

(E) LoD (bottom left) and cooperativity (top right) of double mutants of the D4L base mutant (triple mutants from the WT). Cooperativity = $-\log(LoD_{DM}/LoD_{WT}) - (-\log(LoD_{SM1}/LoD_{WT}) + -\log(LoD_{SM2}/LoD_{WT}))$, where DM refers to the double mutant and SM1 and SM2 to the two corresponding single mutants.

(F) Double mutant cycles. Deviations from the y = x line (gray) indicate non-additivity (cooperativity).

(G) Orthogonal investigation of individual peptide variants with a fluorescence-based plate assay. Antibodies bound to variant peptides (see legend) were challenged for 2 h with varying concentrations of 3×FLAG competitor peptide. Fluorescence values report residual bound M2 antibody.

at other positions in our higher-order mutants. Looking at all double mutants of the only measurable D4 mutant (D4L; triple mutants from WT; Figure 2E), we observe that several combinations of mutations that include D5E and D7K partially rescue D4L, lowering LoD to near-WT levels (Figure 2E). Many of these compensating combinations exhibit significant positive cooperativity (e.g., D4L, D5E, and D7K), demonstrating the ability of Prot-MaP not only to identify critical residues and motifs but also to establish cooperative interaction landscapes that can substantially deviate from simple additive models (Figure 2F).

Interestingly, we also found several FLAG variant sequences that exhibited significantly lower LoD than WT, including a variant we term "superFLAG" (DYKDEDLL), with an extrapolated LoD of 0.14 nM, 7.9-fold lower than WT (Figure 2B). To confirm these

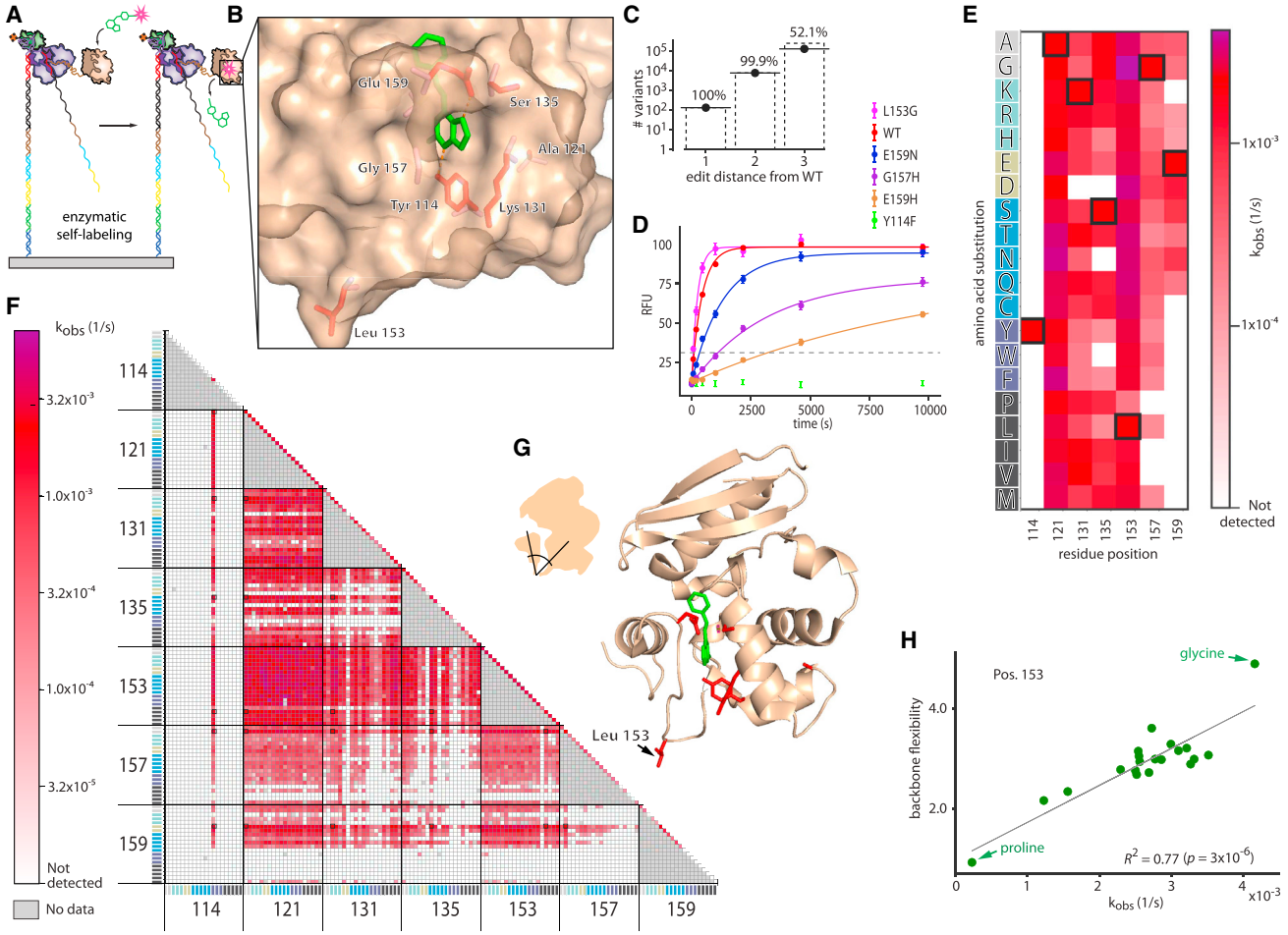

Figure 3. High-Throughput, On-Chip Characterization of Activity across the Mutational Landscape of a Full-Length Enzyme

(A) On-chip SNAP-tag-catalyzed fluorescent self-labeling.

(B) Seven target amino acid positions (red) and benzylguanine substrate (green) on the structure of SNAP-tag (PDB: 3KZZ).

(C) Library coverage of all 19 possible amino acid substitutions in single, double, and triple combinations of the target positions.

(D) Quantified fluorescence medians for selected single mutants (error bars are SEM). Variants that rose above the background threshold (gray dashed) were fit with a single exponential.

(E and F) Fit k_{obs} values for (E) single mutants and (F) double mutants across the 20 amino acids. The WT (unmutated) variant is boxed in black.

(G) Position 153 is in a loop connecting two domains.

(H) Correlation of activity with backbone flexibility (Fuchs et al., 2015) for all 19 amino acid substitutions at position 153. $R^2 = 0.77$ ($p = 3 \times 10^{-6}$ by permutations). Proline is the least flexible and glycine the most flexible.

observations, we performed a fluorescence-based plate assay to measure M2 binding competition between immobilized variant peptides and solutions of 3xFLAG high-affinity peptide (Figure 2G). SuperFLAG displays higher avidity to the M2 antibody then all other assayed peptides, including the original DYKDDDDK immunogen to which M2 was raised (Brizzard et al., 1994).

Unlike chemically synthesized peptide arrays, our *in vitro*-transcribed and -translated array enables the possibility of generating full-length protein features (He et al., 2008; Ramachandran et al., 2004; Tao and Zhu, 2006). To demonstrate this capability, we investigated the mutational landscape of SNAP-tag, an engineered version of O^6-alkylguanine-DNA alkyltransferase, a 181 aa, 20 kD human DNA repair enzyme (Sun et al., 2011). The SNAP-tag protein transfers a benzyl group from a derivatized benzylguanine substrate (often substituted with a fluorophore) to its own Cys 145, thereby covalently labeling itself. The simplicity and specificity of this fluorogenic self-labeling reaction has led SNAP-tag to become widely used as a protein labeling tag, and here it provides an elegant model system for investigation of the sequence-function relationship of an enzyme with Prot-MaP (Figure 3A).

To explore the relationship between protein sequence variation and catalysis in high throughput, we examined the functional interrelationship of seven residues previously identified to modulate function without entirely abolishing catalytic activity (Y114, A121, K131, S135, L153, G157, and E159) (Gautier et al., 2008) (Figure 3B). The DNA sequence encoding this mutated region

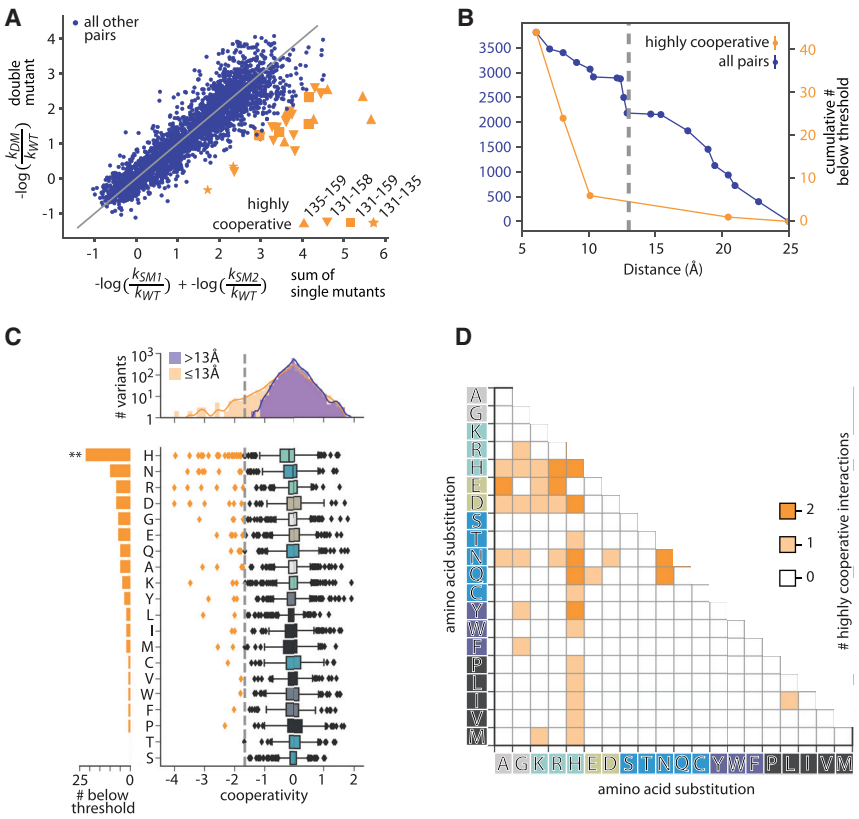

Figure 4. SNAP-Tag Mutational Analysis

(A) Comparison of double mutant effects on activity (y axis) with the sum of single mutant effects (x axis). Only a few residue position pairs (orange) demonstrate high positive cooperativity ("highly cooperative" refers hereafter to cooperativity <−1.69 (see C) where cooperativity = $-\log(k_{obs,DM}/k_{obs,WT}) - (-\log(k_{obs,SM1}/k_{obs,WT}) + -\log(k_{obs,SM2}/k_{obs,WT}))$).

(B) Cumulative number of pairs with C_α–C_α distance within a given distance for highly cooperative (orange), and all target residue pairs (blue).

(C) Most highly cooperative interactions occur within 13 Å (gray dashed). Cooperativity values for all target residue pairs with C_α–C_α distance <13 Å (orange) and >13 Å (blue) (top) and by amino acid (counted for either or both partners) (bottom). Sum of highly cooperative pairs (<−1.69, gray dashed) per amino acid (left).

(D) Number of highly cooperative interactions across all amino acid pairs.

(residues 114–159, the "mutant region") was combinatorially assembled from oligos with the aim of generating single, double, and triple mutant combinations of the 7 target positions across all possible 20 amino acid substitutions (Figure S1). Once assembled, the DNA fragment population was bottlenecked (by diluting to a target number of molecules) and reamplified with PCR to obtain multiple identical copies of molecular variants on the array.

After sequencing this library, RNA synthesis and *in situ* protein generation were performed on the MiSeq flow cell. We then introduced a solution of 200 nM substrate (SNAP-Surface 549) continuously onto the resulting protein array, then measured substrate incorporation over 160 min (see STAR Methods). A total of 6,751,654 clusters were successfully quantified across all time points, and signals were averaged across clusters displaying identical protein variants (>8 clusters per variant). A total of 156,140 unique variants were assayed, including all possible single mutants across all 20 amino acids (133), 7,570 of 7,581 possible double mutants, and 125,076 of 240,065 possible triple mutants (Figure 3C), as well as 23,360 other variants. The majority of mutants (118,025/156,140, 75.59%) exhibited no detectable catalytic activity above background levels, while 32,072 variants exhibited detectable activity that could be well fit by a single exponential to obtain k_{obs} (Figure 3D; see STAR Methods).

We observed large variation in the mutational constraint for each of the 7 targeted amino acids. At one extreme, Y114 is fully constrained to tyrosine across all single and double mutants (Figures 3E and 3F). Even Y114F, a conservative substitution that deletes only a hydroxyl moiety, is inactive (Mollwitz et al., 2012) (Figure 3D), suggesting that the hydrogen bonds that Y114 forms with the benzylguanine substrate are absolutely required for function. While E159 also forms a hydrogen bond with the substrate, a number of mutations to E159 retain measurable activity, suggesting less stringent physicochemical requirements on substrate interactions at this position.

In contrast to these constrained residues, A121 is tolerant to all single mutations. L153 is tolerant to nearly all substitutions, except for proline, which is rotationally constrained in psi and phi Ramachandran angles. By exploring our catalog of double mutants, we observed that proline is consistently the most detrimental of all the 20 amino acids at position 153 across 119/120 other single mutant backgrounds. These observations led to the hypothesis that backbone flexibility at position 153 (which is in the "hinge" region of the loop connecting helix-loop domain 153–176, including the critical residue E159, with the rest of the protein) may regulate activity via inter-domain geometry and/or dynamics (Figure 3G). We investigated this possibility by examining the relationship between the observed enzymatic activity and amino acid backbone flexibility (Fuchs et al., 2015) of amino acid substitutions at position 153. We observed a strong relationship ($R^2 = 0.77$; $p = 3 \times 10^{-6}$; Figure 3H), supporting this hypothesis and highlighting the utility of comprehensive mutational substitutions for testing mechanistic hypotheses.

We next aimed to characterize cooperativity in the interactions between the amino acids we perturbed by analyzing double mutant cycles found within our mutational dataset (Figure 4A). We observe a strong enrichment for physical proximity between highly positively cooperative amino acid pairs, with virtually all strong positively cooperative interactions occurring at C_α–C_α distances less than 13 Å (Figure 4B). For example, many of the

most positively cooperative double mutants are between positions 135 and 159—two amino acids that directly physically interact in the crystal structure (PDB: 3KZZ).

Interestingly, histidine appears particularly amenable to cooperative interactions. Across all positional combinations, histidine was far more likely to form a highly cooperative interaction than any other amino acid (Figure 4C) and did so fairly uniformly with all possible amino acid partners (Figure 4D). Histidine can be either positively charged or neutral in different contexts, can have aromatic character, and can function as both hydrogen bonding donor and acceptor. We hypothesize that histidine may thus function as a "Swiss army knife," pairing in a multifunctional way with diverse partners to produce positive cooperativity. We anticipate that further investigation with high-throughput methods will provide the opportunity to explore this hypothesis in a variety of protein backgrounds.

DISCUSSION

Prot-MaP enables the generation of immense mutational datasets for both peptides and full-length functional proteins directly on a sequencing flow cell, allowing high-throughput analysis of mutational effects based on direct biophysical observations of protein function. Large-scale quantitative measurements of peptide-protein interaction can demonstrate and quantify nonadditivity in affinity landscapes and allow the identification of enhanced-affinity interactions (such as superFLAG). Large-scale functional analysis of full-length proteins allows data-driven characterization of functional networks and cooperative interactions of individual amino acids, geometric constraints that enforce amino acid preferences, and global observations and hypothesis testing regarding the functionality of specific amino acid species (e.g., histidine's observed capacity for widespread cooperative interactions).

Compared to selection methods (e.g., phage display) in which molecular populations can be measured with sequencing over rounds to infer enrichment factors, Prot-MaP has several advantages. First, Prot-MaP allows for direct fluorometric measurements of protein function (e.g., binding), enabling biophysical characterization and eliminating complexities such as amplification bias and stochastic dropout. Second, whereas selections are sophisticated experiments that often take weeks per round to carry out, a Prot-MaP experiment can be performed in a few hours and is highly amenable to automation. Furthermore, while selection-based methods often start from larger libraries of variants, each variant must be sequenced to a relatively high depth to generate quantitative information, whereas every individual cluster (i.e., sequencing read) provides independent information regarding protein function in Prot-Map experiments. Compared to protein and peptide microarrays, Prot-MaP throughput is substantially higher. Prot-MaP can display proteins up to ~200 amino acids in length, while *in situ*-synthesized peptide array platforms are typically limited to ~16 aa or less. Also, protein-coding Prot-MaP DNA libraries can be generated with relatively inexpensive and straightforward synthesis and enzymatic manipulation (e.g., microarray synthesis, doped-base DNA synthesis, and PCR assembly), methods that are substantially much more straightforward and less costly than producing individual peptides and proteins for printing on microarrays. Finally, Prot-MaP is in principle extensible to higher-throughput sequencing platforms, which would enable billions of parallel measurements. As sequencing throughput grows, we anticipate that Prot-MaP has the potential to keep pace by extension.

Limitations

ProtMaP does have limitations, including a practical limit of about 1–2 kb on the length of protein-encoding DNA constructs that can be efficiently clustered and sequenced. These limits are inherited from the underlying sequencing platform and are not intrinsic to the display method. Additionally, many proteins will require different *in vitro* expression conditions and components for efficient production of functional protein (including post-translational modifications). Finally, while binding studies are broadly compatible with fluorescence-based assays, other assays (e.g., for arbitrary enzymatic activities, protein folding, or conformational changes) may necessitate the development of fluorescence-compatible measurement strategies. However, analogous to the many methods built on the foundations of high-throughput sequencing (Morozova and Marra, 2008), we anticipate that the compatibility of Prot-MaP with widely available high-throughput DNA sequencing platforms may serve as a catalyst for further development of specialized applications. For example, comprehensive mutational mapping of the function of disease-associated proteins could enable a deeper understanding of the linkage between mutations and observed clinical pathogenicity. Prot-MaP may also allow characterization and quantification of proteins in complex biological samples such as blood serum using highly multiplexed affinity assays.

Conclusion

The implementation of facile high-throughput protein functional analysis on a broadly available sequencing flow cell demonstrates a conceptually straightforward path toward disseminated high-throughput protein functional assays using automated fluorescence imaging hardware currently used in sequencing by synthesis methods. Given the demonstrated power of high-throughput DNA sequencing methods (as applied through functional genomic methods such as ChIP-seq, Hi-C, etc.) to provide insights into the relationship between DNA sequence and regulatory function, we anticipate that a similarly ubiquitous platform for high-throughput protein assays could have analogous impact on our ability to dissect biologically relevant relationships between protein sequence, structure, and function.

STAR★METHODS

Detailed methods are provided in the online version of this paper and include the following:

- KEY RESOURCES TABLE
- CONTACT FOR REAGENT AND RESOURCE SHARING
- METHOD DETAILS
  - Custom Fluorescence Microscopy Instrument to Interface with MiSeq flow cells ("Imaging Station")
  - Protein Array constructs
  - PCR assembly of constructs

- Ribosomal Stall Sequence
- FLAG Library
- SNAP-tag Library
- Bottlenecking
- Sequencing Diversity
- On-flow cell Polypeptide Array Generation
- M2 Anti-FLAG Antibody Binding Study
- SNAP-tag Enzyme Activity Assay
- Orthogonal investigation of M2/FLAG peptide variant interactions with a fluorescent plate assay

● QUANTIFICATION AND STATISTICAL ANALYSIS
- M2 Anti-FLAG Analysis
- SNAP-tag Analysis

SUPPLEMENTAL INFORMATION

Supplemental Information can be found with this article online at https://doi.org/10.1016/j.molcel.2019.02.019.

ACKNOWLEDGMENTS

We thank Gavin Sherlock, Sarah Denny, Winston Becker, and Sandy Klemm for critical reading of the manuscript. This work was supported by National Institutes of Health (NIH) grant R01-GM111990, P50-HG007735, and UM1-HG009436 and a Technology Development Grant by the Beckman Foundation. W.J.G. is a Chan Zuckerberg Biohub investigator and acknowledges grants 2017-174468 and 2018-182817 from the Chan Zuckerberg Initiative.

AUTHOR CONTRIBUTIONS

Conceptualization: C.J.L. and W.J.G.; Methodology: C.J.L. and W.J.G.; Software: C.J.L. and P.L.M.; Investigation: C.J.L.; Writing – Original Draft: C.J.L. and W.J.G.; Writing – Review & Editing: C.J.L. and W.J.G.; Visualization: C.J.L.; Funding Acquisition: W.J.G.

DECLARATION OF INTERESTS

Stanford University has filed a patent on this work, and C.J.L. and W.J.G. are named as co-inventors.

Received: October 5, 2018
Revised: January 18, 2019
Accepted: February 14, 2019
Published: March 7, 2019

REFERENCES

Bentley, D.R., Balasubramanian, S., Swerdlow, H.P., Smith, G.P., Milton, J., Brown, C.G., Hall, K.P., Evers, D.J., Barnes, C.L., Bignell, H.R., et al. (2008). Accurate whole human genome sequencing using reversible terminator chemistry. Nature *456*, 53–59.

Brizzard, B.L., Chubet, R.G., and Vizard, D.L. (1994). Immunoaffinity purification of FLAG epitope-tagged bacterial alkaline phosphatase using a novel monoclonal antibody and peptide elution. Biotechniques *16*, 730–735.

Buenrostro, J.D., Giresi, P.G., Zaba, L.C., Chang, H.Y., and Greenleaf, W.J. (2013). Transposition of native chromatin for fast and sensitive epigenomic profiling of open chromatin, DNA-binding proteins and nucleosome position. Nat. Methods *10*, 1213–1218.

Buenrostro, J.D., Araya, C.L., Chircus, L.M., Layton, C.J., Chang, H.Y., Snyder, M.P., and Greenleaf, W.J. (2014). Quantitative analysis of RNA-protein interactions on a massively parallel array reveals biophysical and evolutionary landscapes. Nat. Biotechnol. *32*, 562–568.

Chandra, H., Reddy, P.J., and Srivastava, S. (2011). Protein microarrays and novel detection platforms. Expert Rev. Proteomics *8*, 61–79.

Einhauer, A., and Jungbauer, A. (2001). The FLAG peptide, a versatile fusion tag for the purification of recombinant proteins. J. Biochem. Biophys. Methods *49*, 455–465.

Forsström, B., Axnäs, B.B., Stengele, K.-P., Bühler, J., Albert, T.J., Richmond, T.A., Hu, F.J., Nilsson, P., Hudson, E.P., Rockberg, J., and Uhlen, M. (2014). Proteome-wide epitope mapping of antibodies using ultra-dense peptide arrays. Mol. Cell. Proteomics *13*, 1585–1597.

Fowler, D.M., Araya, C.L., Fleishman, S.J., Kellogg, E.H., Stephany, J.J., Baker, D., and Fields, S. (2010). High-resolution mapping of protein sequence-function relationships. Nat. Methods *7*, 741–746.

Fuchs, J.E., Waldner, B.J., Huber, R.G., von Grafenstein, S., Kramer, C., and Liedl, K.R. (2015). Independent metrics for protein backbone and side-chain flexibility: time scales and effects of ligand binding. J. Chem. Theory Comput. *11*, 851–860.

Gautier, A., Juillerat, A., Heinis, C., Corrêa, I.R., Jr., Kindermann, M., Beaufils, F., and Johnsson, K. (2008). An engineered protein tag for multiprotein labeling in living cells. Chem. Biol. *15*, 128–136.

Gu, L., Li, C., Aach, J., Hill, D.E., Vidal, M., and Church, G.M. (2014). Multiplex single-molecule interaction profiling of DNA-barcoded proteins. Nature *515*, 554–557.

Hardesty, B., and Kramer, G. (2001). Folding of a nascent peptide on the ribosome. Prog. Nucleic Acid Res. Mol. Biol. *66*, 41–66.

He, M., Stoevesandt, O., Palmer, E.A., Khan, F., Ericsson, O., and Taussig, M.J. (2008). Printing protein arrays from DNA arrays. Nat. Methods *5*, 175–177.

Hilpert, K., Winkler, D.F., and Hancock, R.E. (2007). Peptide arrays on cellulose support: SPOT synthesis, a time and cost efficient method for synthesis of large numbers of peptides in a parallel and addressable fashion. Nat. Protoc. *2*, 1333–1349.

Jung, C., Hawkins, J.A., Jones, S.K., Jr., Xiao, Y., Rybarski, J.R., Dillard, K.E., Hussmann, J., Saifuddin, F.A., Savran, C.A., Ellington, A.D., et al. (2017). Massively Parallel Biophysical Analysis of CRISPR-Cas Complexes on Next Generation Sequencing Chips. Cell *170*, 35–47.e13.

Kingsmore, S.F. (2006). Multiplexed protein measurement: technologies and applications of protein and antibody arrays. Nat. Rev. Drug Discov. *5*, 310–320.

Krueger, F., Kreck, B., Franke, A., and Andrews, S.R. (2012). DNA methylome analysis using short bisulfite sequencing data. Nat. Methods *9*, 145–151.

Larman, H.B., Zhao, Z., Laserson, U., Li, M.Z., Ciccia, A., Gakidis, M.A., Church, G.M., Kesari, S., Leproust, E.M., Solimini, N.L., and Elledge, S.J. (2011). Autoantigen discovery with a synthetic human peptidome. Nat. Biotechnol. *29*, 535–541.

Legutki, J.B., Zhao, Z.-G., Greving, M., Woodbury, N., Johnston, S.A., and Stafford, P. (2014). Scalable high-density peptide arrays for comprehensive health monitoring.

Levin, A.M., and Weiss, G.A. (2006). Optimizing the affinity and specificity of proteins with molecular display. Mol. Biosyst. *2*, 49–57.

Lieberman-Aiden, E., van Berkum, N.L., Williams, L., Imakaev, M., Ragoczy, T., Telling, A., Amit, I., Lajoie, B.R., Sabo, P.J., Dorschner, M.O., et al. (2009). Comprehensive mapping of long-range interactions reveals folding principles of the human genome. Science *326*, 289–293.

Lipovsek, D., and Plückthun, A. (2004). In-vitro protein evolution by ribosome display and mRNA display. J. Immunol. Methods *290*, 51–67.

Mollwitz, B., Brunk, E., Schmitt, S., Pojer, F., Bannwarth, M., Schiltz, M., Rothlisberger, U., and Johnsson, K. (2012). Directed evolution of the suicide protein O^6-alkylguanine-DNA alkyltransferase for increased reactivity results in an alkylated protein with exceptional stability. Biochemistry *51*, 986–994.

Morozova, O., and Marra, M.A. (2008). Applications of next-generation sequencing technologies in functional genomics. Genomics *92*, 255–264.

Nakatogawa, H., and Ito, K. (2002). The ribosomal exit tunnel functions as a discriminating gate. Cell *108*, 629–636.

Nutiu, R., Friedman, R.C., Luo, S., Khrebtukova, I., Silva, D., Li, R., Zhang, L., Schroth, G.P., and Burge, C.B. (2011). Direct measurement of DNA affinity

landscapes on a high-throughput sequencing instrument. Nat. Biotechnol. *29*, 659–664.

Odegrip, R., Coomber, D., Eldridge, B., Hederer, R., Kuhlman, P.A., Ullman, C., FitzGerald, K., and McGregor, D. (2004). CIS display: In vitro selection of peptides from libraries of protein-DNA complexes. Proc. Natl. Acad. Sci. USA *101*, 2806–2810.

Osada, E., Shimizu, Y., Akbar, B.K., Kanamori, T., and Ueda, T. (2009). Epitope mapping using ribosome display in a reconstituted cell-free protein synthesis system. J. Biochem. *145*, 693–700.

Park, P.J. (2009). ChIP-seq: advantages and challenges of a maturing technology. Nat. Rev. Genet. *10*, 669–680.

Ramachandran, N., Hainsworth, E., Bhullar, B., Eisenstein, S., Rosen, B., Lau, A.Y., Walter, J.C., and LaBaer, J. (2004). Self-assembling protein microarrays. Science *305*, 86–90.

Schaffitzel, C., Hanes, J., Jermutus, L., and Plückthun, A. (1999). Ribosome display: an in vitro method for selection and evolution of antibodies from libraries. J. Immunol. Methods *231*, 119–135.

Seidelt, B., Innis, C.A., Wilson, D.N., Gartmann, M., Armache, J.-P., Villa, E., Trabuco, L.G., Becker, T., Mielke, T., Schulten, K., et al. (2009). Structural insight into nascent polypeptide chain-mediated translational stalling. Science *326*, 1412–1415.

She, R., Chakravarty, A.K., Layton, C.J., Chircus, L.M., Andreasson, J.O.L., Damaraju, N., McMahon, P.L., Buenrostro, J.D., Jarosz, D.F., and Greenleaf, W.J. (2017). Comprehensive and quantitative mapping of RNA-protein interactions across a transcribed eukaryotic genome. Proc. Natl. Acad. Sci. USA *114*, 3619–3624.

Shimizu, Y., Kuruma, Y., Kanamori, T., and Ueda, T. (2014). The PURE system for protein production. In Cell-Free Protein Synthesis: Methods and Protocols, K. Alexandrov and W.A. Johnston, eds. (Humana Press).

Srila, W., and Yamabhai, M. (2013). Identification of amino acid residues responsible for the binding to anti-FLAG™ M2 antibody using a phage display combinatorial peptide library. Appl. Biochem. Biotechnol. *171*, 583–589.

Starosta, A.L., Lassak, J., Peil, L., Atkinson, G.C., Virumäe, K., Tenson, T., Remme, J., Jung, K., and Wilson, D.N. (2014). Translational stalling at polyproline stretches is modulated by the sequence context upstream of the stall site. Nucleic Acids Res. *42*, 10711–10719.

Sun, X., Zhang, A., Baker, B., Sun, L., Howard, A., Buswell, J., Maurel, D., Masharina, A., Johnsson, K., Noren, C.J., et al. (2011). Development of SNAP-tag fluorogenic probes for wash-free fluorescence imaging. ChemBioChem *12*, 2217–2226.

Svensen, N., Peersen, O.B., and Jaffrey, S.R. (2016). Peptide synthesis on a next-generation DNA sequencing platform. ChemBioChem *17*, 1628–1635.

Tao, S.-C., and Zhu, H. (2006). Protein chip fabrication by capture of nascent polypeptides. Nat. Biotechnol. *24*, 1253–1254.

Tome, J.M., Ozer, A., Pagano, J.M., Gheba, D., Schroth, G.P., and Lis, J.T. (2014). Comprehensive analysis of RNA-protein interactions by high-throughput sequencing-RNA affinity profiling. Nat. Methods *11*, 683–688.

Ude, S., Lassak, J., Starosta, A.L., Kraxenberger, T., Wilson, D.N., and Jung, K. (2013). Translation elongation factor EF-P alleviates ribosome stalling at polyproline stretches. Science *339*, 82–85.

Yin, J., Straight, P.D., McLoughlin, S.M., Zhou, Z., Lin, A.J., Golan, D.E., Kelleher, N.L., Kolter, R., and Walsh, C.T. (2005). Genetically encoded short peptide tag for versatile protein labeling by Sfp phosphopantetheinyl transferase. Proc. Natl. Acad. Sci. USA *102*, 15815–15820.

Zykovich, A., Korf, I., and Segal, D.J. (2009). Bind-n-Seq: high-throughput analysis of in vitro protein-DNA interactions using massively parallel sequencing. Nucleic Acids Res. *37*, e151.

STAR★METHODS

KEY RESOURCES TABLE

REAGENT or RESOURCE	SOURCE	IDENTIFIER
Antibodies		
Monoclonal ANTI-FLAG M2 antibody produced in mouse	Sigma	F1804; RRID: AB_262044
Goat Anti-Mouse IgG H&L (Alexa Fluor 555) preadsorbed	Abcam	ab150118; RRID: AB_2714033
Goat Anti-Mouse IgG Fc (DyLight 550) preadsorbed	Abcam	ab98713; RRID: AB_10672339
Chemicals, Peptides, and Recombinant Proteins		
3X FLAG Peptide	Sigma	F4799
Deposited Data		
FLAG-tag and SNAP-tag high-throughput Prot-MaP mutational datasets	Mendeley Data	https://doi.org/10.17632/49rf4xfk8k.1
Software and Algorithms		
Image analysis software	Buenrostro et al., 2014	http://www.nature.com/articles/nbt.2880
Hardware control software	GreenleafLab GitHub	https://github.com/GreenleafLab/ImagingStationController

CONTACT FOR REAGENT AND RESOURCE SHARING

Further information and requests for resources and reagents should be directed to and will be fulfilled by the Lead Contact, William Greenleaf (wjg@stanford.edu).

METHOD DETAILS

Custom Fluorescence Microscopy Instrument to Interface with MiSeq flow cells ("Imaging Station")

We developed a custom instrument with all the core functionality of a sequencer that interfaces with a MiSeq flow cell, as well as software methods to align sequence reads to image features (see Supplemental Information). This platform has been described previously (She et al., 2017) but briefly, the camera, lasers, z-stage, x-y stage, syringe pump, and objective lens salvaged from Illumina GAIIx instruments were combined with custom laser control electronics, retrofitted temperature control, and a fluidic interface designed to be compatible with the MiSeq flow cell.

Protein Array constructs

To generate a protein array, engineered DNA constructs (Figures 1 and S1) were constructed to have the elements necessary for sequencing on an unmodified Illumina MiSeq, principally the sequencing adapters P5 and P7 and sequencing primer hybridization sites. After clustering and sequencing on the MiSeq, the sequenced flow cell was moved to our custom platform, where transcription/translation was performed on chip such that both the transcript and nascent peptide remain associated with their DNA template, producing a tethered protein array. Library constructs therefore contain the elements requisite for prokaryotic *in vitro* transcription and translation, in addition to those that enable tethered display. These include an RNAP promoter and stall sequence that allow generation of a tethered RNA substrate with one-RNAP-per-template as previously described (Buenrostro et al., 2014). To allow generation of polypeptide, constructs contain a Shine-Dalgarno ribosomal binding site to initiate translation followed by a start codon. The polypeptide library of interest is encoded at the N-terminal end of the translated sequence. After this coding region, the open reading frame (ORF) continues with no stop codon via a short linker to a spacer polypeptide (2x ybbR tag (Yin et al., 2005)). A spacer is necessary to display the protein/peptide of interest (POI) away from the ribosome where it can be accessible to interaction and, in the case of longer proteins, fold correctly (Schaffitzel et al., 1999). Sufficient linker sequence is present to ensure that the nascent POI and spacer become accessible outside the ribosome exit tunnel (Hardesty and Kramer, 2001). Next, a ribosome stall sequence that we engineered for maximum stalling efficiency (see Figure S2) stalls ribosomal progress, allowing robust display of the nascent peptide (Figure 1). Fluorescence-based functional assays (here, measuring binding of a fluorescently labeled partner or the enzymatic incorporation of fluorescent substrates) may then be carried out directly on this generated array.

PCR assembly of constructs

All PCR assembly was performed with NEBNext High-Fidelity 2X PCR Master Mix (NEB) using the recommended reaction setup and thermocycling conditions.

Ribosomal Stall Sequence

Highly stable, efficient ribosomal stalling is critical for generating high-quality peptide arrays. We achieve stalling with a ribosome stall sequence (CJL-PPP) that we rationally designed based on polyproline translational pausing in a maximally efficient context (Starosta et al., 2014). This sequence produces a strong pausing signal in our *in vitro* translation mix that does not contain Elongation Factor P (EF-P) (which alleviates stalling at the PPP motif) (Ude et al., 2013) nor Release Factor 1 (RF1), which would allow release at the Amber stop codon that immediately follows the polyproline stretch. To further stabilize this display, critical residues from SecM and TnaC that are presumed to promote stalling via direct interaction with the exit tunnel (F150, W155, I156 from SecM (Nakatogawa and Ito, 2002), and W12, D16 from TnaC (Seidelt et al., 2009)) were also transplanted into the CJL-PPP sequence (Figure S2A). In our (RF-1-free) translation mix, The CJL-PPP stall sequence produces much more efficient display than a simple Amber stop codon with no stall sequence (Figure S2B).

FLAG Library

Each residue in the 8-amino acid WT FLAG peptide sequence (DYKDDDDK) is substituted with 6 different amino acids (A,K,D,S,F, and L, representing small, positive, negative, polar, aromatic, and aliphatic substitutions, respectively). If the wild-type identity of the residue at that position is already one of the mutation set, a contingency substitution (V,R,E,T,Y, or I) was made in lieu of a redundant mutation. The library consists of all combinations of single, double, and triple substitutions of these 6 mutations at each position using optimal codons for *E. coli*. 2xFLAG (DYKDDDDKGDYKDHD, the first two FLAG motif repeats of the commonly used 3xFLAG sequence) was also included in the library. Designs were synthesized on microarray (CustomArray) with flanking primer regions, then assembled by PCR into the full-length protein array construct (Figure S1).

SNAP-tag Library

Seven amino acid positions in the SNAP-tag sequence chosen for their involvement in substrate specificity (Y114, A121, K131, S135, L153, G157, and E159) (Gautier et al., 2008) were targeted for mutation. Most of these residues, except A121 and L153 are peristeric to the active site. The 138-base mutant region from 114-159, as well as the sequencing primer regions 31 bases upstream and 31 bases downstream, were covered with three overlapping oligos that could be combinatorially assembled. Oligos were obtained (IDT) with all combinations of wild-type and NNK codons at each mutant position. The first primer covered positions 114 and 121, the second 131 and 135, and the third 153, 157, and 159. Assembly reactions for each single (7 reactions), double (21 reactions), and triple (35 reactions) combination of positions were individually assembled (Figure S1), quantified, and pooled so that the final library representation was 1% single mutants, 5% double mutants, and 94% triple mutants.

Additional constructs spanning the mutant region were also included in the final sequencing library. One encodes the WT region with no mutations, and another NNK codons at all 7 targeted positions. These were spiked in downstream at low percentage, along with the fiducial marks.

Bottlenecking

In order to have each molecular variant represented multiple times on chip, protein array libraries were bottlenecked down to 33fM (FLAG library) and 300fM (SNAP library) in 0.1% tween-20, then reamplified. The ~1kb SNAP library constructs were gel extracted from a 1.5% agarose gel to ensure length homogeneity.

Sequencing Diversity

As with all Illumina sequencing, it is necessary to ensure sufficient sequence diversity in the sequenced region. FLAG peptide constructs were sequenced together with other, unrelated libraries that added sequencing diversity (e.g., ATAC-seq samples). However, because the SNAP-tag constructs are ~1kb in size, a diversity element of matched length (and therefore clustering efficiency) was specifically constructed. This diversity element has randomized N78-mer sequence across the entire mutant region, but is otherwise identical to the protein array constructs. Because the SNAP-tag library contains stretches that are essentially homogeneous, this diversity element was spiked in at up to 40%.

On-flow cell Polypeptide Array Generation

Libraries were prepared for sequencing on a MiSeq by first precisely quantifying all concentrations with qPCR and/or TapeStation (Agilent), then spiking in fiducial mark constructs into protein array libraries at 0.5%–1%. Fiducial marks are sparse library members that serve as hybridization targets for a fluorescent probe; the resulting pattern is used to orient the chip relative to the sequencing data on the imaging station platform. Other library constructs, including the specifically designed SNAP-tag diversity elements, were also present in the pooled sequencing sample to add sufficient sequence diversity for high-quality sequencing.

Standard amplicon sequencing was performed for FLAG tag peptide variants. For the ~1kb SNAP-tag variant library, a modified "Long Amplicon" sequencing recipe with more clustering cycles was used. In order to make these modifications, the "Amplicon" XML recipe in the MiSeq control software was modified to increase the bridge PCR "Repeat" cycles in "Amplification 1" during initial "OnBoardClusterGeneration" from 24 to 32, as well as the "Repeat" cycles in "Resynthesis" during "PairedEndTurnaround" from 12 to 16.) Sequencing was then performed with custom construct-specific sequencing primers (the read1 primer is the 31-base sequence immediately preceding the mutant region, and the read2 primer is the reverse complement of the 31-base

sequence immediately following the mutant region). After sequencing, the sequenced MiSeq flow cell is moved to our custom imaging station.

On the Imaging Station platform, residual primers or read fragments from sequencing are stripped off with 100% formamide at 55°C. Cy3-labeled fiducial mark probes in hybridization buffer (5x SSC, 5mM EDTA, 0.01% Tween-20) are then hybridized to the fiducial marks (60°C for 15 min, 40°C for 12 min). Fiducial mark probes remain hybridized as reference points throughout the experiment.

Though the MiSeq flow cell has clusters along the length of its continuous channel, during the course of sequencing the MiSeq only collects data at a series of tiled locations. Experimental images must be taken at the same tile positions in order to match the imaged clusters to the sequence data. In order to discover these tile locations and program their relative positions on a new instrument, images from the imaging station are registered to the fiducial mark construct locations identified from the sequencing data with cross-correlation. MiSeq flow cells have two imaging surfaces (top and bottom) with a typical throughput of 20-25 million reads total. Because the current implementation of our imaging station only images the bottom of the flow cell and obstructs the objective lens from imaging the last (19^{th}) tile, we typically make 10-12 million individual measurements across bottom tiles 1-18. Therefore, given our requirement for 8 replicates per variant, and that our experimental setup images only 47.3% of the flowcell, the theoretical maximum diversity for the existing setup is approximately ($25x10^6$ / 8)*(0.473) = ~1.5M variants – assuming a library of perfectly uniform abundance of each molecular variant). Using a slightly modified imaging infrastructure capable of imaging the whole flowcell, we estimate our throughput would be ~3.1M

Once registered to the sequencing data, tethered RNA transcript is generated on chip as described previously (Buenrostro et al., 2014) by stalling *E. coli* RNA polymerase on a DNA templates (clusters) with a terminal streptavidin roadblock. Constructs are washed with PBST +$MgCl_2$ (137 mM NaCl, 2.7 mM KCl, 8 mM Na_2HPO_4, 2 mM KH_2PO_4, 0.05% Tween-20, 7mM $MgCl_2$), then prokaryotic ribosomes are initiated on the transcript, which contains a Shine-Dalgarno sequence, with the PURExpress (Shimizu et al., 2014) *in vitro* translation mix. The PURExpress system is reconstituted from purified components and lacks EF-P (Ude et al., 2013) allowing ribosomes to stall at a polyproline-containing ribomsome stall sequence that we engineered into the library, stably displaying the nascent peptide. We used a custom PURExpress formulation that omits Release Factors 1, 2, and 3 as well as T7 RNA polymerase, CTP, and UTP. Not only are these transcriptional components unnecessary (as the RNA template is already generated and displayed before adding the translation reagents) they interfered with stable nascent peptide display in this system despite the lack of a T7 promoter on our constructs.

Translation was performed for 1 hour at 37°C. After peptide display, the flow cell was washed with PBST +$MgCl_2$. All buffers post-RNA generation, including the translation mix, contain 0.8 U/μL Superase-In RNase inhibitor (Thermo AM2696).

M2 Anti-FLAG Antibody Binding Study

After generation of the peptide array, nonspecific binding sites were blocked with bind buffer (0.8% BSA and 500nM goat IgG in PBST +$MgCl_2$) for 30min at 25°C. All subsequent binding steps were performed at 25°C. 35nM Alexa555-goat anti-mouse secondary antibody (Abcam ab150118) in bind buffer was then incubated for 37 min so that the initial, zero-primary-antibody-concentration point would show any background binding of secondary antibody as baseline. Each experimental concentration of primary antibody (1nM, 3.2nM, 10nM, 32nM, 100nM) was incubated for 45 min, followed by a 25 min wash with bind buffer, then detected with a 37 min incubation with 35nM Alexa555-goat anti-mouse secondary antibody in bind buffer, and a 25 min wash with bind buffer. After each experimental concentration, tiles on the bottom side of the flow cell were TIRF imaged at 532nM excitation with a 590/104 nm bandpass (Semrock FF01-590/104-25) emission filter, using the same laser power and camera exposure settings across all concentrations.

Continuous flow at 12.5 μL/min was used in lieu of static incubation for low-nM primary Ab concentrations to mitigate depletion.

SNAP-tag Enzyme Activity Assay

SNAP-tag substrate SNAP-surface 549 (NEB #S9112) was dissolved in DMSO to a stock concentration of 1μM, then was diluted immediately before use to a working concentration of 200nM in PBST +$MgCl_2$. After generation of the protein array, the working solution of SNAP substrate was flowed continuously into the flow cell at 12.5μL/min for the experimental incubation times to minimize substrate depletion or product inhibition. At each imaging time point, fresh PBST +$MgCl_2$ was flowed in as an imaging buffer, and tiles on the bottom side of the flow cell were TIRF imaged at 532nM excitation and a 590/104 nm bandpass (Semrock FF01-590/104-25) emission filter. (Cumulative reactions times include only incubation time in the presence of substrate, not imaging buffer).

Orthogonal investigation of M2/FLAG peptide variant interactions with a fluorescent plate assay

To test M2 antibody binding to these variant peptides orthogonally from Prot-MaP, an *in vitro* plate assay was performed. First, several 8-amino acid variants of the FLAG peptide were individually synthesized followed by the context amino acids DHDGS (identical to the 5 downstream amino acids of the on-chip constructs) and a C-terminal PEG-biotin. A neutravidin-coated plate (Pierce 15117) was washed, then blocked with StartingBlock PBS (Thermo 37538). Biotinylated peptides were then bound to the plate by incubating for 30 min at a concentration of 5nM. After washing, primary antibody (M2 anti-FLAG, Sigma F1804) was incubated in the plate for 30 min, then washed, then fluorescently labeled (DyLight 550) goat Anti-Mouse secondary antibody (Abcam ab98713) was incubated for 1 hour, then washed again. In order to observe differential binding, a concentration gradient of 3xFLAG peptide (Sigma F4799) competitor in PBST +$MgCl_2$ was added and allowed to equilibrate for 2 hours, after which the plate was washed and read at 535(25) nm excitation and 580(30) nm emission. (Antibodies and peptides were diluted in StartingBlock PBS + 0.05% Tween-20, all washes and fluorescence measurements were performed with PBST +$MgCl_2$, and all incubations were performed at 4°C with shaking.)

Note in Figure 2G that, though approximate rank order is maintained between the plate assay and Prot-MaP results, while the D4L rescue mutant (D4L, D5E, D7K) is observed to exhibit nearly WT LoD by Prot-MaP (1.09nM versus 1.05nM, respectively), it shows significantly lower binding than WT in the presence of 3xFLAG competitor in the plate assay. The observed differences may reflect different underlying biophysical interactions between competition in the plate and on-chip. For example, re-binding mechanics of bivalent antibody avidity are likely different between the two assays, given the presence of competitor and differences in peptide surface density between assays.

QUANTIFICATION AND STATISTICAL ANALYSIS

Fluorescence images, paired with cluster sequence identities and positions from the sequencing run, are quantified to measure fluorescent signal, and therefore assay the fluorescence-reported polypeptide or protein function at each cluster.

After imaging, fine registration of the images to the sequencing data is necessary before image quantification due to microscope stage position inaccuracy and, more onerously, potentially non-affine optical aberrations between the sequencing platform and the imaging station. To address this, each image is divided into a grid of sub-images that are individually registered to the data, followed by a fit of the offset positions to a 2D quadratic surface. The resulting continuous offset map is then applied to the data to achieve fine registration of cluster positions to the images (She et al., 2017).

Images are then quantified by fitting small image subtiles to a summation of 2D Gaussians centered at the sub-pixel registered positions of each cluster. Edge effects in quantification are mitigated by discarding fit values close enough to an edge to be affected by out-of-bounds clusters, and using overlapping subtiles to completely cover the image (Buenrostro et al., 2014). The integrated intensity of each Gaussian is reported as the fluorescence value for each cluster.

To correct for small variances in quantified intensity caused by inconsistent focus and/or illumination power fluctuation, median fluorescence values were normalized to the median intensity of the fiducial marks. Protein expression/display efficiency is not directly normalized. Variation in our overall signal from stochastic cluster-to-cluster protein display was minimized by using the median signal from 8 or more clusters encoding identical variants. However, we note that sequence-specific differences in protein expression could be conflated with protein function in interpreting observed signals. We plan to implement translation-level normalization in the future.

Data from quantified images are consolidated across concentrations on a per-cluster basis. The resulting experimental series are then grouped into molecular variants with identical amino acid sequences. Grouping into variants was handled slightly differently for the FLAG and SNAP experiments. For FLAG variants, a 16-base random unique molecular identifier (UMI) was read (as index read 2) and the consensus sequence of the amino acid-coding region determined for each UMI was used. SNAP library constructs did not have a UMI sequence and the raw coding sequence was used. For all variants represented by some minimum number of clusters (here, 8), median fluorescence values were calculated at each experimental time point, which were then used for downstream analysis (Figure S3). Variant medians in this study are aggregated across a single-flow-cell experiment.

M2 Anti-FLAG Analysis

A threshold of detection was defined by a set of negative control peptide sequences. The negative set consists of all variants represented by 8-or-more clusters where residues D1, Y2, and K3 (each individually critical for binding) were all mutated in combination. The threshold was then defined as 3σ above the mean of the fluorescence medians of this negative set. Encouragingly, fluorescent signal from the negative set did not appreciably increase with increasing concentration of primary antibody, so the median value of the negative set across all concentration points was used as a concentration-independent background threshold.

This threshold of detection served as the basis for quantification of variant LoD. Any variant that did not cross the threshold was classified as "negative" (LoD greater than the highest the assay can measure).

For variants with 4-or-more points above threshold, the points above threshold (only) were fit to a line and the intersection of the line with the threshold value was reported as the LoD. For variants with fewer than 4 points above threshold, a linear interpolation was done between the point before and the point after crossing the threshold (Figure 2B).

SNAP-tag Analysis

A threshold of detection was defined by a set of negative control enzyme variants. The negative set consists of all well-represented variants where all seven targeted residues (Y114, A121, K131, S135, L153, G157, E159) were mutated in combination. The threshold was then defined as 3.3σ above the mean of the negative set medians across concentration points.

All variant medians that rose above threshold by the second-to-last time point were fit by unconstrained nonlinear least-squares to a single exponential:

$$F = F_{min} + F_{max}\left(1 - e^{-k_{obs}t}\right)$$

Quality control (QC) of fits was evaluated by three criteria: (1) $R^2 > 0.70$, (2) F_{max} above background threshold (3) $F_{min} < F_{max} < \text{threshold}_{Fmax}$ (see Figure S4). Variants that did not meet these criteria were excluded from downstream analysis.